Mechanical Systems and Signal Processing 103 (2018) 89–104

Contents lists available at ScienceDirect

Mechanical Systems and Signal Processing

journal homepage: www.elsevier.com/locate/ymssp

A guided wave dispersion compensation method based on compressed sensing

Cai-bin Xu [a], Zhi-bo Yang [a], Xue-feng Chen [a,*], Shao-hua Tian [b], Yong Xie [c]

[a] School of Mechanical Engineering, Xi'an Jiaotong University, Xi'an 710049, China
[b] Collaborative Innovation Center of High-end Manufacturing Equipment, Xi'an Jiaotong University, Xi'an 710049, China
[c] School of Aerospace, Xi'an Jiaotong University, Xi'an 710049, China

ARTICLE INFO

Article history:
Received 16 June 2017
Received in revised form 11 September 2017
Accepted 29 September 2017

Keywords:
Dispersion compensation
Guided wave
Compressed sensing
Sparse representation
Structural health monitoring

ABSTRACT

The ultrasonic guided wave has emerged as a promising tool for structural health monitoring (SHM) and nondestructive testing (NDT) due to their capability to propagate over long distances with minimal loss and sensitivity to both surface and subsurface defects. The dispersion effect degrades the temporal and spatial resolution of guided waves. A novel ultrasonic guided wave processing method for both single mode and multi-mode guided waves dispersion compensation is proposed in this work based on compressed sensing, in which a dispersion signal dictionary is built by utilizing the dispersion curves of the guided wave modes in order to sparsely decompose the recorded dispersive guided waves. Dispersion-compensated guided waves are obtained by utilizing a non-dispersion signal dictionary and the results of sparse decomposition. Numerical simulations and experiments are implemented to verify the effectiveness of the developed method for both single mode and multi-mode guided waves.

1. Introduction

Ultrasonic guided waves, such as Lamb waves, have received considerable attention because of their powerful properties, such as high sensitivity to various types of damage, and the capacity of monitoring a large area while a sparse sensor array is used for damage detection. Therefore, guided waves appear to be very crucial in nondestructive testing (NDT) [1,2] and structural health monitoring (SHM) [3–5]. In the past decades, many important applications of guided waves in engineering are proposed in various fields. Some examples including aluminum structures [6,7], pipes/axles [8], and carbon fiber reinforced composite laminates [9–11] have validated the effectiveness of the guided wave based method for damage detection. In the field of guided wave based SHM, a common system configuration uses a sparse array of mounted or embedded sensors in structures to excite or record guided waves. In most SHM damage detecting algorithms, such as delay-and-sum (DAS) [12] method, minimum variance distortionless response (MVDR) [13] method, and correlation-based [14,15] methods, the reference guided waves should be acquired to serve as the baseline for damage detection. Therefore, only the residual signals, the results of subtracting the baseline signals from the recorded signals, are used in those algorithms.

The guided waves registered from structures, for example, aluminium plates, are usually complicated. Except the portions caused by the geometric characteristics, such as edge reflections, there exist at least two guided wave modes at any

* Corresponding author.
E-mail address: chenxf@mail.xjtu.edu.cn (X.-f. Chen).

https://doi.org/10.1016/j.ymssp.2017.09.043
0888-3270/

frequency in plate like structures, known as multi-mode characteristic. Furthermore, since the frequency dependence of guided wave velocities, even in a plate of equal thickness, the recorded guided waves will disperse either in time or space, which is referred to as dispersion. When the propagation distance increases, the dispersion effect will be more serious. As the consequence of multi-mode and dispersion effect, the wave packets will overlap with each other degrading the temporal resolution of the guided waves and making the signals hard to be interpreted. For multi-mode, dispersion effect can be compensated or suppressed by selecting the special excitation center frequency [16] or using a mode selection technique [17–19]. Therefore, the methods of dispersion compensation or dispersion removal should be developed.

The simplest method to suppress the dispersion is to use narrowband excitation [20], usually a windowed tone burst centered at a certain frequency. In such frequency bandwidth, the group velocity is small fluctuation with respect to frequency. However, the time width and frequency bandwidth cannot be decreased simultaneously. When frequency bandwidth decreases, the dispersion effect decreases, but the temporal resolution also decreases. Furthermore, the dispersion effect will increase when propagation distance increases. Wilcox [21] proposed a rapid signal processing technique to compensate the dispersion effect by making use of a priori knowledge of the dispersion curves of the structure, which is referred to as the time-distance mapping method. It transforms the dispersive guided waves from time domain to frequency domain, then interpolates to wavenumber domain and finally maps signals to distance domain. The method is based on the fact that the dispersion compensated signals can be obtained by propagating backward the recorded signals to its source. Although it is a popular dispersion compensation method, the waveform of each wave packet after compensated is deformed and not identical with the original excitation. Liu and Yuan [22] proposed a linear mapping technique for dispersion removal based on Taylor linear approximation of wavenumber. The linear mapping performed the dispersive signals in wavenumber domain to transform the nonlinear dispersion relation into the linear one by truncating the Taylor expansion into linear term which is nondispersive. Xu et al. [26] compared the above two methods, dispersion compensation(the time-distance mapping method) and dispersion removal, and drew a conclusion that the dispersion removal method outperformed the dispersion compensation method but the former was not able to directly get the spatial locations of the wave packets. De Marchi et al. [23,24] presented a guide wave dispersion compensation method, referred to as the warped frequency transform (WFT), which maps frequency domain into "frequency warped" domain by a warping function. However, the compensated signal is still deformed compared with the excitation because of the nonlinearity of the warping function [25]. Recently, Luo et al. [27] analyzed the reason of waveform deformation in the time-distance mapping method, and developed a reshaped excitation dispersion compensation method by generating a reshaped excitation. The reshaped excitation was carefully developed according to the original excitation and group velocity. However, the above methods only work efficiently under the situation that only one mode exists in wave propagation. For multi-mode cases, the target mode guided waves can be compensated completely, but the non-target modes will be compensated partly or become even more dispersive.

As a theory of having the capability to deal with signal sparse decomposition and reconstruction, compressed sensing (CS) [28,29] has attracted great interest in the field of guided wave based signal processing. Based on the sparse prior of the guided waves in a specified dictionary, some sparse reconstruction algorithms have been developed to process guided waves. Mor et al. [30] proposed a support matching pursuit (SMP) method for approximating overlapping ultrasonic echoes based on a Gabor dictionary. The results showed that the SMP method can separate overlapping echoes, and it can achieve superior performance than matching pursuit (MP) and basis pursuit (BP) method. Tse and Wang [31] used MP for reconstruction of defect reflection signals in pipes with an optimized dictionary based on two interfering reflection. Harley and Moura [32] showed the capability of the orthogonal matching pursuit (OMP) in recovering dispersion curves from guided wave data. Mesnil and Ruzzene [33] developed a CS technique through $l1$-minimization for the sparse reconstruction of guided wavefields. In [34], Perelli et al. proposed a WFT based CS method for guide wave damage localization. Through this method, the sparse reflectivity function in distance domain can be recovered from the dispersive guided waves, which improves the accuracy of wave propagation distance estimation. In [35], Perelli et al. used the WFT and wavelet packet to generate the best basis for a sparse representation of dispersive guided waves. In [36], De Marchi et al. used a BP algorithm combined with a warped dictionary, which has the potential to match each mode guided waves, to extract the distance of guide wave propagation. Through building different sparse representation models and constructing the corresponding dictionaries, different results can be achieved for guided waves, such as feature extraction, wavefield reconstruction, and echo separation, as mentioned above.

To address the problem of dispersion compensation for both single mode and multi-mode guide waves, a new method based on CS is presented in this paper. This method leverages the assumption of sparsity of the number of wave packets with respect to the number of sampling points, and uses the powerful sparse decomposition and reconstruction techniques to implement dispersion compensation. In order to implement sparse decomposition, the developed method builds a dispersion signal dictionary by utilizing the dispersion characteristic of the guided wave modes firstly. Each atom of the dispersion signal dictionary corresponds to a dispersive guided wave which dispersively propagates a certain distance. Secondly, the compensated guided waves are reconstructed using the results of sparse decomposition and a non-dispersion signal dictionary, which is built by the non-dispersion relation of the inspected structure. Results show that the developed method can compensate the dispersive guided waves for both single mode and multi-mode.

The following sections are organized as follows. In Section 2, the time-distance mapping method is reviewed and discussed. In Section 3, the methodology of the proposed dispersion compensation method is presented. The numerical simulation and experimental verification are presented in Sections 4 and 5, respectively. In Section 6, conclusions are given.

2. Review of the dispersion compensation method

In this section, the classical time-distance mapping dispersion compensation method is reviewed for the sake of completeness, and the phenomenon of waveform deformation is also presented and analyzed.

2.1. Dispersion effect on guided waves

An ideal plate with constant thickness is investigated here. The guided waves propagating in a plate, known as Lamb waves, can be predicted neglecting amplitude change and scattering. Suppose only single Lamb mode is excited, the response Lamb wave $u(x,t)$ between two points can be expressed as [21]

$$u(x,t)=\frac{1}{2\pi}\int_{-\infty}^{+\infty}F(\omega)e^{j\omega t}e^{-jkx}d\omega, \tag{1}$$

where $F(\omega)$ is the Fourier transform of the excitation $f(t)$, x is the distance between the two points, $k=k(\omega)$ is the wavenumber of the Lamb mode. If k and ω are linear relationship, the envelope of response signal $u(x,t)$ will have the same waveform with the original excitation $f(t)$. While in practice, the nonlinear property of $k(\omega)$ will lead to dispersion.

2.2. Time-distance mapping method

For a special recorded signal $y_0(t)$ with a propagating distance x_0, $y_0(t)$ can be predicted by the following equation neglecting its amplitude change

$$y_0(t)=u(x,t)|_{x=x_0}=\frac{1}{2\pi}\int_{-\infty}^{+\infty}F(\omega)e^{j(\omega t-kx_0)}d\omega. \tag{2}$$

Eq. (2) suggests that one can simulate a dispersive Lamb wave after propagating a certain distance.

Based on the fact mentioned above, the time-distance mapping method is proposed in [21]. As its name suggests, the goal of the time-distance mapping dispersion compensation method is to transform a signal from time domain into distance domain and implement dispersion compensation simultaneously. The dispersion compensated signal $y(x)$ can be obtained by back propagating (which means that the propagation distance is equal to $-x$) the recorded signal $y_0(t)$ to its excitation source (where $t=0$). Thereafter, the distance domain signal $y(x)$ can be written as

$$y(x)=u(x,t)|_{\substack{x=-x\\t=0}}=\frac{1}{2\pi}\int_{-\infty}^{+\infty}Y_0(\omega)e^{jkx}d\omega, \tag{3}$$

where $Y_0(\omega)$ is the Fourier transform of the recorded time domain signal $y_0(t)$. It is not efficient to implement Eq. (3) directly. Note that the variables of distance x and wavenumber k hold as a Fourier transform pair, just like the variables of time and frequency. Therefore, one can transform the variable of frequency ω into wavenumber k by the definition of group velocity $c_g(\omega)$

$$d\omega=c_g(\omega)dk. \tag{4}$$

Substitute Eq. (4) into Eq. (3), the dispersion compensated signal $y(x)$ is equal to

$$y(x)=\frac{1}{2\pi}\int_{-\infty}^{+\infty}Y_0(\omega)c_g(\omega)e^{jkx}dk=\frac{1}{2\pi}\int_{-\infty}^{+\infty}G(k)e^{jkx}dk, \tag{5}$$

where $G(k)=G(\omega(k))=Y_0(\omega)c_g(\omega)$ uses the relationship of dispersion characteristic (ω,k), and it can be obtained by interpolating. Eq. (5) can be implemented by the inverse fast Fourier transform (IFFT).

2.3. Wave packet deformation

In order to investigate the waveform of the dispersion compensated wave packet with respect to the original excitation, rewrite Eq. (2) in frequency domain as

$$Y_0(\omega)=F(\omega)H(\omega), \tag{6}$$

where $H(\omega)=e^{-jkx_0}$ is the system response from the transmitter location to the receiver location. Using Fourier transform, one can get the system response in distance domain as

$$h(x)=\frac{1}{2\pi}\int_{-\infty}^{+\infty}H(k)e^{jkx}dk=\frac{1}{2\pi}\int_{-\infty}^{+\infty}e^{-jkx_0}e^{jkx}dk=\delta(x-x_0), \tag{7}$$

where $H(k)$ can be obtained from $H(\omega)$ by interpolation using the (ω,k) relation. Eq. (7) suggests that the system response $h(x)$ does not change the waveform of a wave packet with respect to the excitation in distance domain. Substitute Eq. (6) into Eq. (5), one can get

$$y(x) = \frac{1}{2\pi}\int_{-\infty}^{+\infty} F(\omega)c_g(\omega)H(\omega)e^{ikx}dk = \frac{1}{2\pi}\int_{-\infty}^{+\infty} F_1(k)H(k)e^{ikx}dk, \tag{8}$$

and

$$y(x) = f_1(x) * h(x), \tag{9}$$

where $F_1(k) = F(\omega)c_g(\omega), H(k) = H(\omega), \omega = \omega(k)$, and $f_1(x)$ is the inverse Fourier transform of $F_1(k)$. Substitute Eq. (7) into Eq. (9), one can get

$$y(x) = f_1(x) * \delta(x - x_0) = f_1(x - x_0). \tag{10}$$

Eq. (10) suggests that the dispersion compensated signal $y(x)$ is a constant distance shifting with respect to $f_1(x)$. However, $f_1(x)$ is not identical with $f(x)$. $f_1(x)$ is deformed with respect to the original excitation $f(x)$ because of the relation $F_1(k) = F(\omega)c_g(\omega)$. In other words, there is nonlinear scaling in the process of interpolating $F_1(\omega) = F(\omega)c_g(\omega)$ into $F_1(k)$ and amplitude modulation by the nonlinear function $c_g(\omega)$. Fortunately, the deformation after the time-distance mapping is only related to the dispersion characteristic $k(\omega)$ and group velocity $c_g(\omega)$, but independence of propagation distance. As an example, Fig. 1(b) shows a simulated A0 mode dispersive Lamb wave in an aluminum plate with three wave packets, with propagation distances of 200 mm, 280 mm, and 500 mm, respectively. Their amplitudes are 1, 0.5, and 0.2, respectively. Fig. 1(c) shows the result using the time-distance mapping method. The excitation is a Hanning-windowed tone burst with 3 cycles and 80 kHz center frequency, as shown in Fig. 1(a). The compensated results of the time-distance mapping method for the three wave packets hold the same waveform but are not identical with the original excitation. As analyzed above, the dispersion compensated signal after time-distance mapping is deformed and independent of propagation distance.

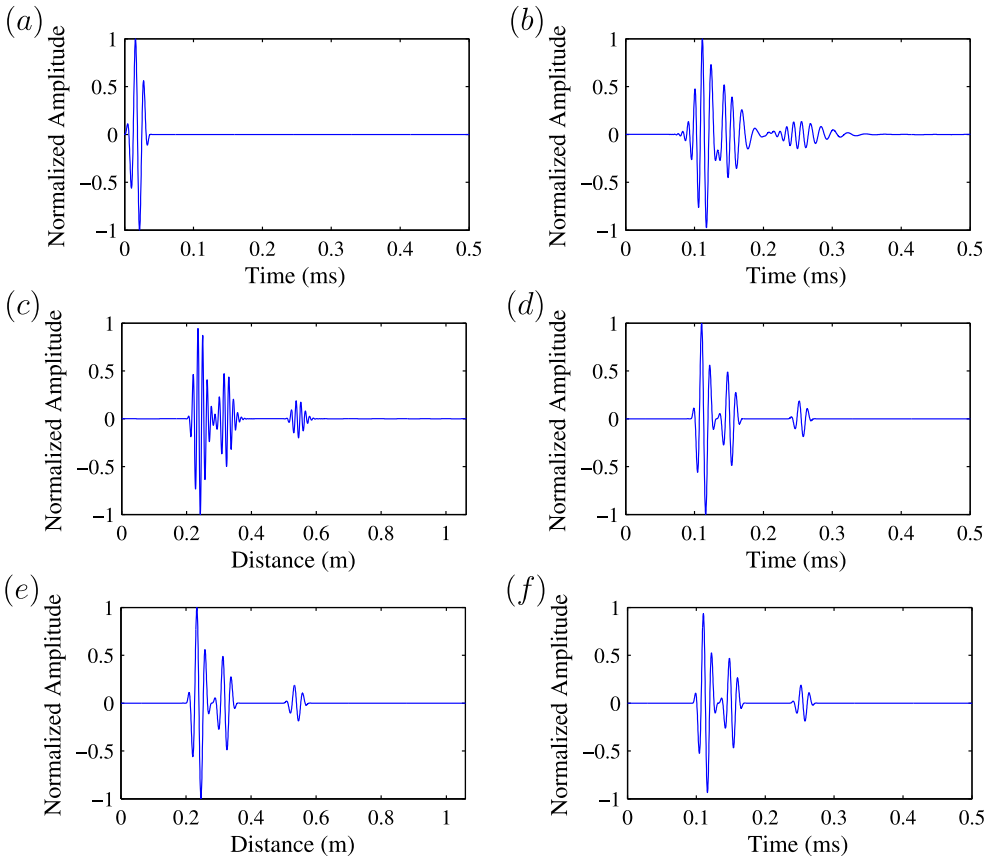

Fig. 1. Numerical simulation of dispersion compensation of 80 kHz A0 mode on a 2-mm aluminum plate: (a) 3-cycle Hanning-windowed tone burst excitation centered at 80 kHz; (b) the simulated recorded signal containing three wave packets with the propagation distances of 200 mm, 280 mm, and 500 mm; (c) compensated result using the time-distance mapping method; (d) compensated result using the developed method; (e) result transformed into distance domain from (d); (f) the non-dispersive signal (ground truth) in time domain.

3. Methodology of the developed method

In order to address the problem illustrated above, a novel guided wave dispersion compensation method is proposed. The developed method performs well for single-mode or multi-mode cases as the effect of CS theory introduced in the presented methodology. This section is organized in a progressive manner. The dispersive guided wave is decomposed in a carefully built dictionary based on the compressed sensing theory, which is also known as the sparse decomposition. The dispersion compensated guided wave can be obtained by the non-dispersion dictionary and the result of sparse decomposition. The similar procedure is finally extended to the multi-mode cases using the multi-mode dictionaries.

3.1. Signal sparse decomposition in a dispersion dictionary

Considering the amplitude factor and multi-source scattering, which results in multi-wave packets problem, the recorded signal in Eq. (2) can be modified as

$$s_0(t) = \sum_j \frac{A_j}{2\pi} \int_{-\infty}^{+\infty} F(\omega) e^{j(\omega t - k x_j)} d\omega = \sum_j A_j u(x_j, t), \tag{11}$$

where x_j is the propagation distance of the jth wave packet, and A_j is the corresponding amplitude factor. In vector notation, Eq. (11) can be written as

$$\mathbf{s}_0 = [\mathbf{u}_1,\ \mathbf{u}_2, \ldots,\ \mathbf{u}_j, \ldots][A_1,\ A_2, \ldots,\ A_j, \ldots]^{\mathrm{T}}, \tag{12}$$

where $\mathbf{u}_j$ is the vector notation of $u(x_j, t)$. In Eq. (12), the amplitude factor vector $[A_1,\ A_2, \ldots,\ A_j, \ldots]^{\mathrm{T}}$ represents the weight of each wave packet but does not localize the time of flight (TOF) of the wave packet in time domain. Therefore, we modify the matrix $[\mathbf{u}_1,\ \mathbf{u}_2, \ldots,\ \mathbf{u}_j, \ldots]$ in the following part so as to make the amplitude factor vector $[A_1,\ A_2, \ldots,\ A_j, \ldots]^{\mathrm{T}}$ have the information of TOF.

Suppose that $\mathbf{u}_i$ is of length M, then the propagation distance is discretized to N values with the same sampling frequency of $\mathbf{u}_i$. The ith value can be written as

$$x_i = c_g(f_c) t_i = c_g(f_c) \frac{i}{f_s}, \quad i \in [0,\ N-1], \tag{13}$$

where $c_g(f_c)$ is the group velocity at center frequency f_c, f_s is the sampling frequency of the recorded signal $s_0(t)$, and i is a integer. So the recorded signal $\mathbf{u}_i$ corresponding to the propagation distance x_i can be written as

$$\mathbf{u}_i = u(x_i, t) = \frac{1}{2\pi} \int_{-\infty}^{+\infty} F(\omega) e^{j\omega t} e^{-jkx_i} d\omega. \tag{14}$$

Thereafter, a dictionary can be built using $\mathbf{u}_i$ in a linear combination

$$\mathbf{U} = [\mathbf{u}_0,\ \mathbf{u}_2, \ldots,\ \mathbf{u}_i, \ldots \mathbf{u}_{N-1}]\mathbf{D}^{-1}, \tag{15}$$

where $\mathbf{D} \in \mathbb{R}^{N \times N}$ is a diagonal matrix with elements $\mathbf{D}_{i,i} = \|\mathbf{u}_i\|_2$, which normalizes the columns of $\mathbf{U}$ to unit 2-norm. The $\mathbf{U}$ is an $M \times N$ matrix, which is referred to as dispersion dictionary in this paper. The corresponding amplitude factor vector can be written as

$$\mathbf{a} = [A_0, A_1, \ldots,\ A_i,\ \ldots,\ A_{N-1}]^{\mathrm{T}}. \tag{16}$$

We can represent the actual recorded signal $\mathbf{s}_0$ using the dispersion dictionary $\mathbf{U}$ and the corresponding amplitude factor vector $\mathbf{a}$

$$\mathbf{s}_0 = \mathbf{U}\mathbf{a}. \tag{17}$$

Note that the amplitude factors in Eq. (16) and in Eq. (12) are not identical. In Eq. (16), most of the amplitude factors are zeros because the number of wave packets is far less than the recording length in usual, which means that the $\mathbf{a}$ in Eq. (16) is sparse. If the element A_i in $\mathbf{a}$ is nonzero, then it mean that $\mathbf{s}_0$ has a component of signal $\mathbf{u}_i$ with an amplitude of A_i and a TOF of $t_i = i/f_s$. Therefore, the nonzero values in $\mathbf{a}$ not only represent the amplitude factors, but also carry the TOF information of the corresponding wave packets.

Considering additive noise $\mathbf{w}$ in Eq. (17), we have

$$\mathbf{s}_0 = \mathbf{U}\mathbf{a} + \mathbf{w}. \tag{18}$$

Because of the sparsity of $\mathbf{a}$, the solution of Eq. (18) can be found using $l1$-optimization method [28]. The problem in Eq. (18) can be treated as a basis pursuit denoising (BPD) problem [37], which can be written as a constrained optimization problem

$$\arg\min_{\mathbf{a}} \|\mathbf{a}\|_1 \text{ subject to } \|\mathbf{s}_0 - \mathbf{U}\mathbf{a}\|_2^2 \leqslant \sigma^2, \tag{19}$$

or a unconstrained optimization problem

$$\arg\min_{\mathbf{a}} \frac{1}{2}||\mathbf{s}_0 - \mathbf{U}\mathbf{a}||_2^2 + \lambda||\mathbf{a}||_1, \tag{20}$$

where $||\mathbf{a}||_1 = \sum_{i=0}^{N-1}|A_i|, 0 \leqslant \sigma \leqslant ||\mathbf{s}_0||_2$, and $\lambda \in (0, \max|\mathbf{U}^{\mathrm{T}}\mathbf{s}_0|]$ is a regularization parameter that balances 2-norm term (accuracy) and 1-norm term (sparsity). In this paper, λ is set to be $\lambda_{\max}/10 = \max|\mathbf{U}^{\mathrm{T}}\mathbf{s}_0|/10$. The problem of Eq. (20) can be solved by many algorithms for convex optimization, e.g. spectral projected-gradient (SPG) algorithm [38,39], and split variable augmented Lagrangian shrinkage algorithm (SALSA) [40,41].

3.2. Signal reconstruction in a non-dispersion dictionary

In order to get the non-dispersive signal, the wavenumber k is linearized to k'

$$k'(\omega) = \frac{1}{c_g(2\pi f_c)}\omega. \tag{21}$$

Then we can get the corresponding phase velocity $c_p(\omega)$ and the group velocity $c_g(\omega)$

$$c_p(\omega) = \frac{\omega}{k'} = c_g(2\pi f_c), \tag{22}$$

$$c_g(\omega) = \frac{d\omega}{dk'} = c_g(2\pi f_c). \tag{23}$$

Substitute Eqs. (22) and (13) into Eq. (2), the recorded $M \times 1$ non-dispersive signal $y_i(t)$ can be written as

$$y_i(t) = \frac{1}{2\pi}\int_{-\infty}^{+\infty} F(\omega)e^{j(\omega t - k'x_i)}d\omega = \frac{1}{2\pi}\int_{-\infty}^{+\infty} F(\omega)e^{j\omega(t-t_i)}d\omega = f(t-t_i). \tag{24}$$

Eq. (24) shows that the non-dispersive signal is equal to a time-shifted excitation. A non-dispersion dictionary $\mathbf{U}'$ can be built using $y_i(t)$ in a linear combination

$$\mathbf{U}' = [y_0(t),\ y_1(t),\ \ldots, y_i(t),\ \ldots, y_{N-1}(t)]\mathbf{D}'^{-1}, \tag{25}$$

where $\mathbf{U}' \in \mathbb{R}^{M\times N}$, and $\mathbf{D}' \in \mathbb{R}^{M\times N}$ is a diagonal matrix with elements $\mathbf{D}'_{i,i} = \|y_i(t)\|_2$, which normalizes the columns of $\mathbf{U}'$ to unit 2-norm. Fig. 2 shows an intuitive explanation of the dispersion and non-dispersion dictionaries, namely $\mathbf{U}$ and $\mathbf{U}'$.

Finally, the dispersion compensation signal $\hat{\mathbf{s}}_0$ can be obtained by

$$\hat{\mathbf{s}}_0 = \mathbf{U}'\hat{\mathbf{a}}, \tag{26}$$

where $\hat{\mathbf{a}}$ is the solution of Eq. (20). To sum up, the following two main steps are implemented in order to obtain the compensated signal:

Step 1: Signal sparse decomposition based on the dispersion dictionary

$$\arg\min_{\mathbf{a}} \frac{1}{2}||\mathbf{s}_0 - \mathbf{U}\mathbf{a}||_2^2 + \lambda||\mathbf{a}||_1. \tag{27}$$

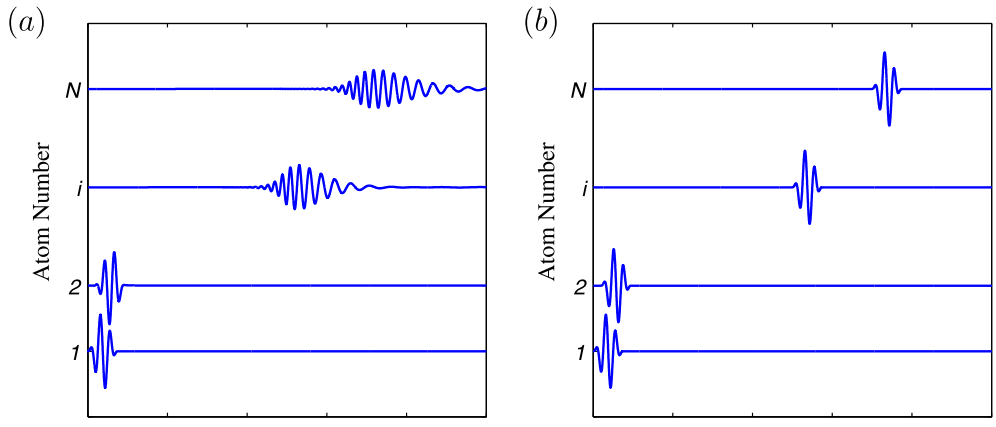

Fig. 2. An intuitive explanation of the two dictionaries. (a) The dispersion dictionary, (b) the non-dispersion dictionary.

Step 2: Signal reconstruction based on the non-dispersion dictionary

$$\hat{\mathbf{s}}_0 = \mathbf{U}'\hat{\mathbf{a}}. \tag{28}$$

3.3. Dispersion compensation for multi-mode guided waves

The above contents in this section present the procedures for single mode guided waves dispersion compensation. To extent the method to multi-mode cases, we combine the corresponding single mode dictionary one by one to build a multi-mode dictionary. For example, if the recorded signal contains two Lamb modes, A0 and S0, we should combine the A0 and S0 mode dictionaries together. As a result, the dispersion and non-dispersion dictionaries for A0 and S0 modes are written as

$$\mathbf{U} = [\mathbf{U}_{A0}, \mathbf{U}_{S0}], \tag{29}$$

$$\mathbf{U}' = [\mathbf{U}'_{A0}, \mathbf{U}'_{S0}], \tag{30}$$

where the columns of $\mathbf{U}_{A0}, \mathbf{U}_{S0}, \mathbf{U}'_{A0}$, and $\mathbf{U}'_{S0}$ have been normalized to unit 2-norm. Then implement the above two steps, the multi-mode compensated signal can be obtained. The developed method can be described by the flowchart illustrated in Fig. 3.

4. Numerical simulation

Numerical simulations for single mode and multi-mode guided wave dispersion compensation are implemented in this section to validate the effectiveness of the developed method. Serving as the baseline and benchmark, the compensation results given by the time-distance mapping method are also presented for comparison. The numerical simulations are implemented on a 2-mm aluminum plate ($\rho = 2690$ kg/m^3, $E = 68.9$ GPa, $\sigma = 0.33$) containing two wave modes (A0 and S0). The group velocity and phase velocity dispersion curves are calculated by the Global Matrix Method (GMM) algorithm [42], as shown in Fig. 4. It should be noticed that the presented conclusion can be easily extended to more complicated cases.

4.1. Dispersion compensation for single mode guided waves

To highlight the dispersion effect according to the dispersion curves, the excitation is selected to be a 3-cycle Hanning-windowed tone burst centered at 80 kHz for A0 mode and at 1 MHz for S0 mode.

Simulation results of the A0 mode are shown in Fig. 1. Fig. 1(c) and (d) shows the compensated results of the time-distance mapping and the developed methods, respectively. For a direct visual comparison, the result in Fig. 1(d) is transformed into distance domain, as shown in Fig. 1(e), using the group velocity at center frequency $c_g(f_c)$. The non-dispersive wave packets after propagation are shown in Fig. 1(f), which can be used as the ground truth. The non-dispersive wave packets are obtained by taking the group velocity as a constant $c_g(f_c)$. Both of the two methods can recover the signal interfered by dispersion effect. The result of the developed method performs better as the recovered waveform of every wave packet is closer to the original excitation, while the time-distance mapping method deforms the waveform of the corresponding wave packet.

Simulation results of the S0 mode are shown in Fig. 5. The results are similar with the case of the A0 mode, and the similar conclusions can be obtained. The main difference between Figs. 1 and 5 is that the resolution of the compensated signal in Fig. 5 is improved in both time and distance domain because higher excitation frequency leads to shorter wavelength.

4.2. Sensitivity

The accurate dispersion curves are hard to access in practice due to the uncertainties of the inspected structures. Therefore, the sensitivity of the compensation methods to inaccurate dispersion curves is crucial, and thus it is analyzed in this section. Two different cases with the vertical axis data (group or phase velocity) perturbation and horizontal axis data (frequency) perturbation are investigated for further validation. The sensitivity analysis is based on the S0 mode waves centered at 1 MHz, in which the dispersion curves change rapidly. The corresponding results of the time-distance method can be found in [21].

Case 1: Vertical axis data perturbation in dispersion curves.

In this case, the vertical axis data is perturbed with respect to the accurate vertical data. Taking group velocity as an example, the perturbed data can be written as

$$c'_g(f) = (1 + \alpha)c_g(f), \tag{31}$$

where $c'_g(f)$ and $c_g(f)$ are the perturbed and the accurate group velocities, $\alpha$is a constant factor, which controls the degree of perturbation. When the group velocity changes, the corresponding phase velocity and wavenumber also change

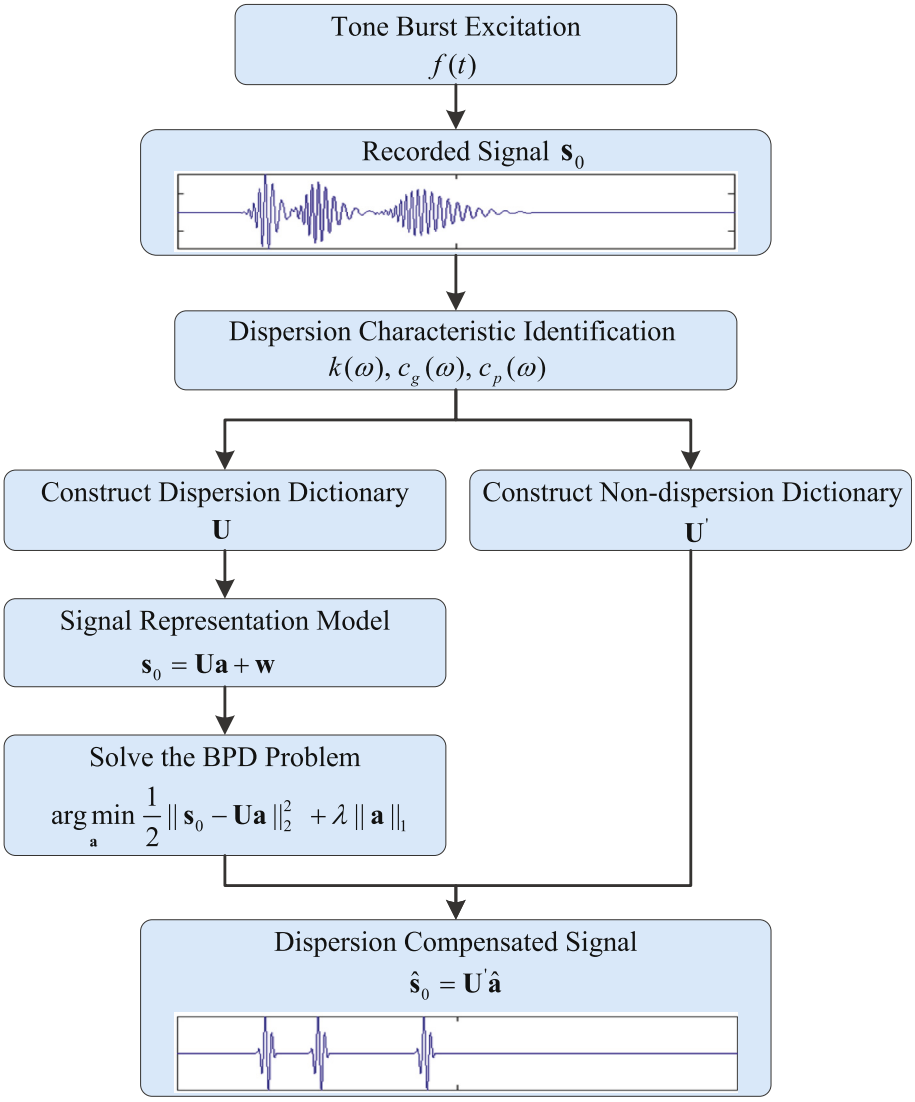

Fig. 3. Schematic of the process of the developed method for dispersion compensation.

$$c_p'(f) = (1+\alpha)c_p(f), \tag{32}$$

$$k'(f) = (1+\alpha)k(f). \tag{33}$$

In this case, the waveforms of the dispersion curves do not change but shift along vertical axis, as shown in Fig. 4. The perturbation of vertical data may happen in the case of using inaccurate parameters of material properties to calculate the dispersion curves. The compensated results for a dispersive signal containing two wave packets with propagation distances of 100 mm and 200 mm, are presented in Fig. 6(b)–(d). As the results show, the compensated waveforms in Fig. 6 (b)–(d) are almost identical, which means that the proposed method is robust to the vertical axis perturbation. The non-dispersive wave packets after propagation are shown in Fig. 7(a), which can be used as the ground truth. Note that, the compensated signals in Fig. 6(b)–(d) are corresponding to three different group velocities, which means that they are corresponding to three different propagation distances.

Case 2: Horizontal axis data perturbation in dispersion curves.

In this case, the frequency data perturbation is investigated. Assuming frequency changes with a perturbation factor β in frequency axis, namely $f' = (1+\beta)f$, one can write the dispersion characteristic as

$$k'(f) = k((1+\beta)f), \tag{34}$$

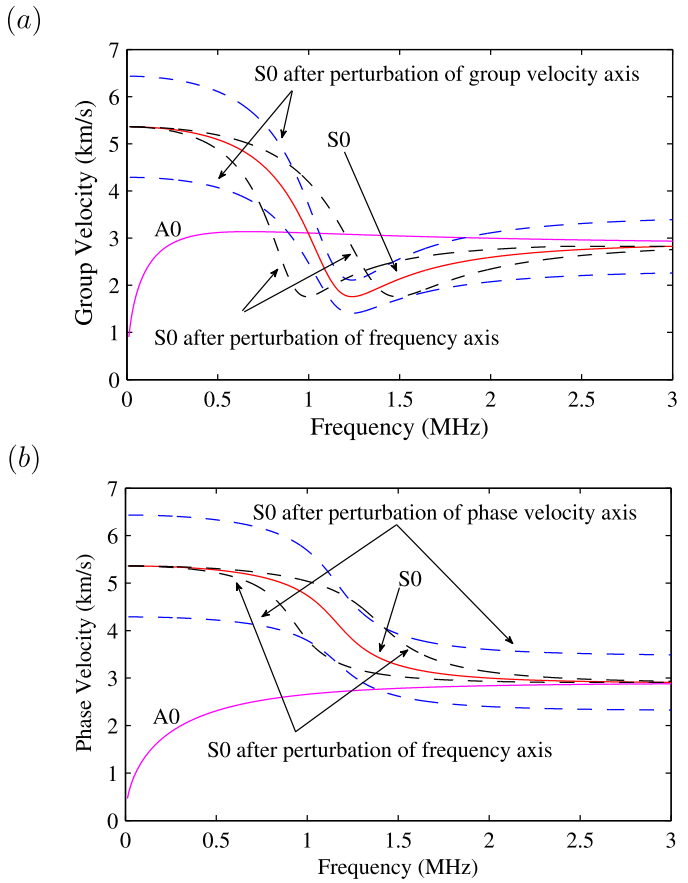

Fig. 4. Dispersion characteristic of a 2-mm aluminum plate: (a) group velocity, and (b) phase velocity, showing the perturbations applied to the S0 mode.

$$c'_g(f) = c_g((1+\beta)f), \tag{35}$$

$$c'_p(f) = c_p((1+\beta)f). \tag{36}$$

In this case, the outlines of the dispersion curves are changed, as shown in Fig. 4. This perturbation may happen in the case of inaccurate physical thickness of the plate [21]. The corresponding compensated results for Fig. 6(a) are shown in Fig. 7(b)–(d). As displayed in Fig. 7(b)–(d), the frequency perturbation has a great influence on the compensated results. Compared with the uncompensated signal, as shown in Fig. 6(a), the compensated signals can suppress the dispersion effect even with perturbation factor $\beta = \pm 0.2$ to some extent.

4.3. Dispersion compensation for multi-mode guided waves

Dispersion compensation for multi-mode guided waves is validated in this part. A simulated modes (A0 and S0) dispersive signals are generated to test the developed method, as shown in Fig. 8(a). The original excitation is a 3-cycle Hanning-windowed tone burst centered at 300 kHz. As shown in Fig. 8(a), the dispersive signal contains two mode components with different propagation distances, 300 mm for A0 mode and 600 mm for S0 mode, and the two wave packets overlap together. The corresponding compensated results by the time-distance mapping method using the S0 and A0 mode dispersion curves are presented in Fig. 8(b) and (c), respectively. In the case of multi-mode, one mode can be compensated completely but the other mode can be incompletely compensated or even more dispersive when the time-distance mapping method is employed for compensation. As the compensated results show, the time-distance mapping method cannot deal with the cases of multi-mode dispersive signals. However, the developed method can completely compensate every mode component to the original excitation well, as shown in Fig. 8(d). The corresponding non-dispersive signals (ground truth) in distance domain and in time domain are shown in Fig. 8(e) and (f), respectively.

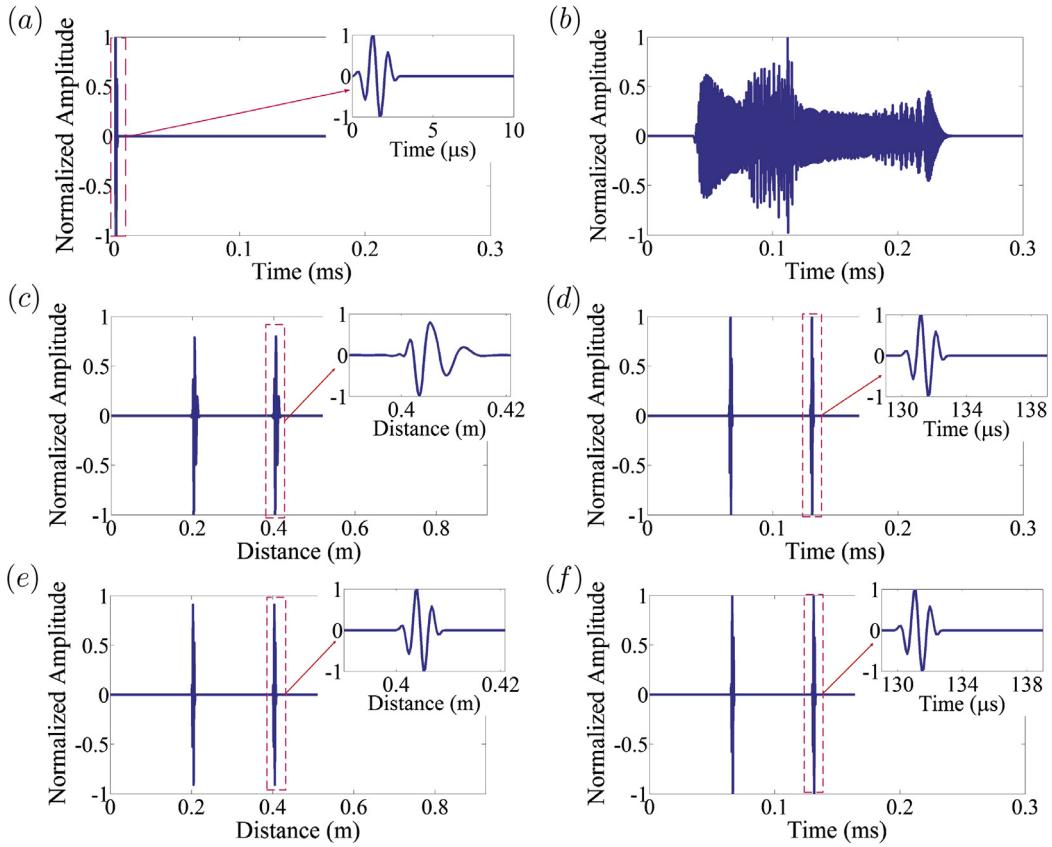

Fig. 5. Numerical simulation of dispersion compensation of 1 MHz S0 mode on a 2-mm aluminum plate: (a) 3-cycle Hanning-windowed tone burst excitation centered at 1 MHz; (b) the simulated recorded signal containing two wave packets with the propagation distances of 200 mm and 400 mm; (c) compensated result using the time-distance mapping method; (d) compensated result using the developed method; (e) the non-dispersive signal (ground truth) in distance domain; (f) the non-dispersive signal (ground truth) in time domain.

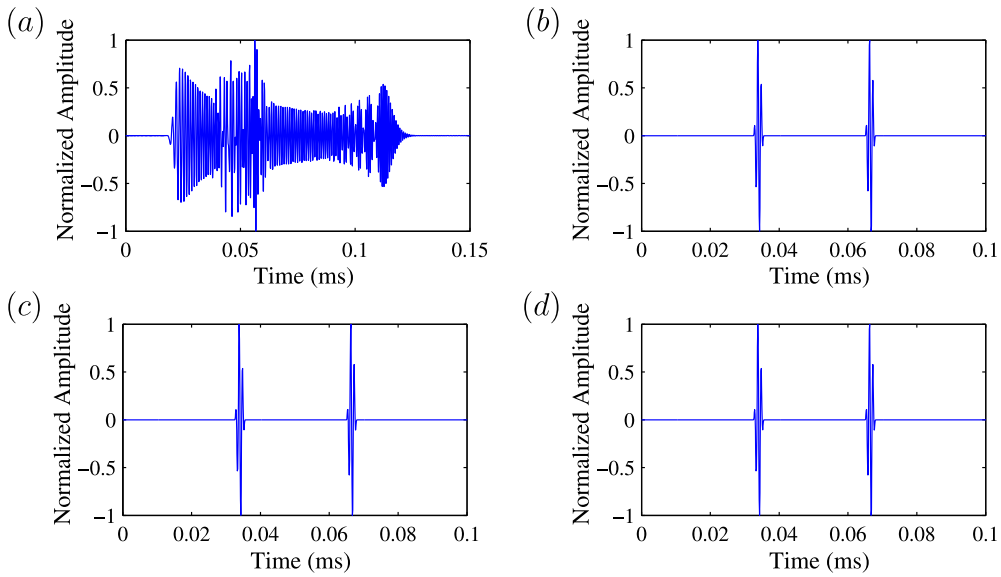

Fig. 6. Dispersion compensated results for a dispersive signal containing two wave packets with propagation distances of 100 mm and 200 mm. (a) The uncompensated signal; the results using the developed method with perturbation factor α equal to (b) −0.2, (c) 0, (d) 0.2.

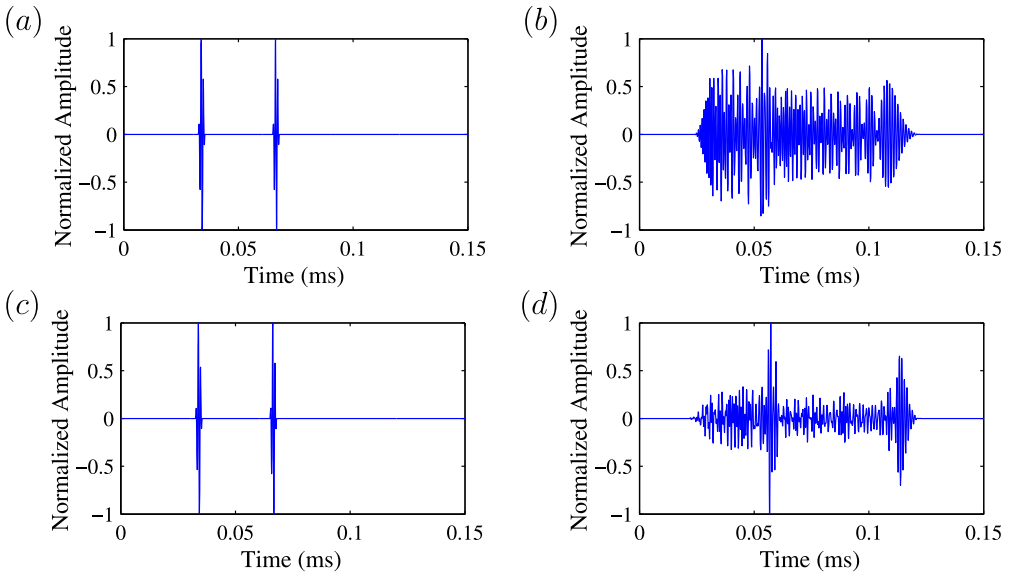

Fig. 7. Dispersion compensated results for Fig. 6(a). (a) The non-dispersive signal (ground truth); the results using the developed method with perturbation factor β equal to (b) -0.2, (c) 0, (d) 0.2.

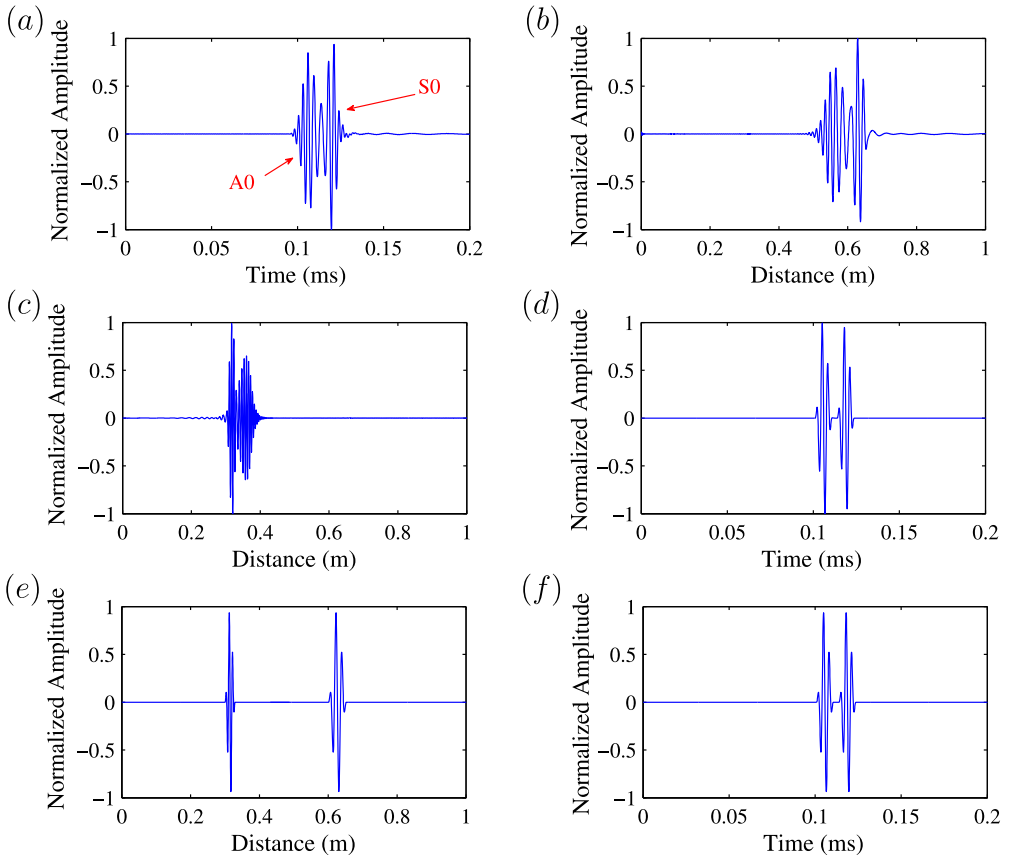

Fig. 8. Numerical simulation of dispersion compensation of 300 kHz two modes, A0 and S0, on a 2-mm aluminum plate: (a) the simulated dispersive signal which contains A0 and S0 mode components with the propagation distance of 300 mm and 600 mm, respectively; (b) compensated result of the time-distance mapping method using the S0 mode dispersion curves; (c) compensated result of the time-distance mapping method using the A0 mode dispersion curves; (d) compensated result of the developed method; (e) the non-dispersive signal (ground truth) in distance domain; (f) the non-dispersive signal (ground truth) in time domain.

4.4. Discussion

In the case of dispersion compensation for multi-mode guided waves, sparse decomposition for the dispersive signal in Eq. (27) is based on the corresponding multi-mode dispersion dictionary. In order to completely compensate all the dispersive modes, the dispersion dictionary must contain all the corresponding modes. Otherwise, the dispersive signal will be incompletely compensated, or even more dispersive. To test performance of the proposed method in the case of incomplete dispersion dictionary, a case study is implemented here for a simulated dispersive signal containing A0 and S0 mode components, as shown in Fig. 9(a). The compensated results using only A0 or S0 mode dispersion dictionary are shown in Fig. 9 (b) and (c), respectively. In Fig. 9(b), the dispersive signal of the S0 mode component is compensated, while the A0 mode component is almost uncompensated. In Fig. 9(c), the dispersive signal of the A0 mode component is compensated, while the S0 mode component is more dispersive than the original. For a comparison, the compensated result using multi-mode (A0 and S0) dispersion dictionary is also presented, as shown in Fig. 9(d). In conclusion, the proposed CS based dispersive compensation model cannot handle the case of incomplete dispersion dictionary. But usually in practice, one can know in advance the components contained in the dispersive signal and then construct the dispersion dictionary according to the components.

In the proposed method, the regularization parameter in Eq. (27) is specified to be $\lambda = \lambda_{\max}/10$. The dispersive signal containing three wave packets, as shown in Fig. 1(b), are added SNR = 10 dB Gaussian noise and then used to test the influence of the regularization parameter λ on the amplitude after dispersive compensation. The three wave packets from left to right in Fig. 1(b) are denoted as s1, s2, s3. The value of λ has a significant influence on the compensated results, especially the envelope amplitudes of the compensated wave packets, as shown in Fig. 10. The actual envelope amplitudes of the three wave packets after dispersion compensation mainly decrease as the regularization parameter λ increases. The smaller value of the regularization parameter λ, the more iterations and computing time it takes. The more noise, the lager of λ should be specified. In this paper, we specify $\lambda = \lambda_{\max}/10$ as taking into account noise.

5. Experimental verification

In this section, dispersion compensation is implemented by the developed method for the actual dispersive signals recorded on a 2-mm aluminum plate. The mechanical parameters of the aluminum plate are the same with that used in numerical simulation. The experimental setup and transducers arrangements are shown in Fig. 11. The transducers are PZT disks with 0.5 mm thickness and 8 mm diameter. The single mode and multi-mode cases are investigated independently. In the case of single mode, the center frequency of the excitation can be changed to obtain a dominant guided wave mode according to the wavelength tuning effect [43]. All the other modes except the dominant mode are treated as noise in single mode case. The corresponding results by the time-distance mapping method are also presented for comparison.

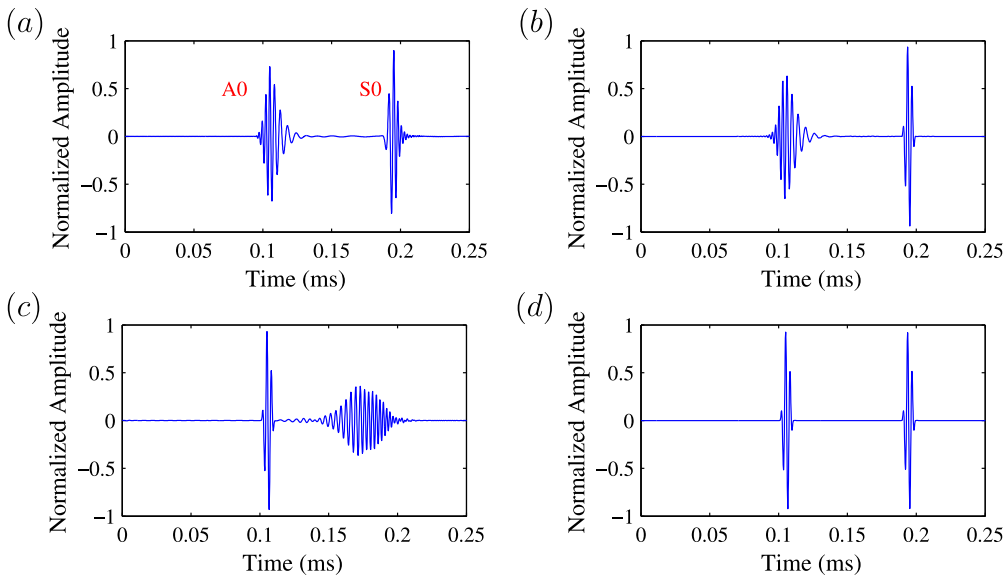

Fig. 9. Performance of incomplete dispersion dictionary. (a) the simulated dispersive signal which contains A0 and S0 mode components with the propagation distances of 300 mm and 1000 mm, respectively; (b) compensated result of the proposed method using only S0 dictionary; (c) compensated result of the proposed method using only A0 dictionary; (d) the compensated result of the proposed method using multi-mode (A0 and S0) dispersion dictionary.

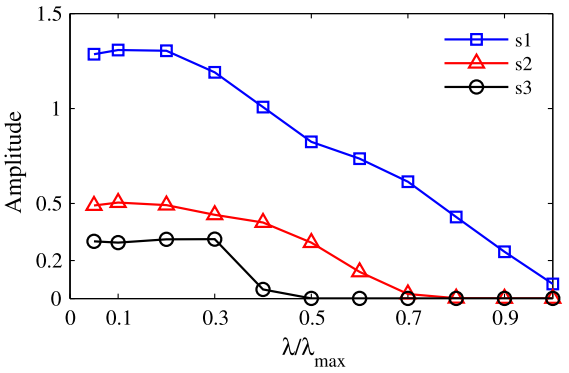

Fig. 10. Envelope amplitudes of the three compensated wave packets as a function of the regularization parameter for the proposed method. s1, s2, s3 represent the compensated wave packets for the three wave packets in Fig. 1(b), from left to right, respectively.

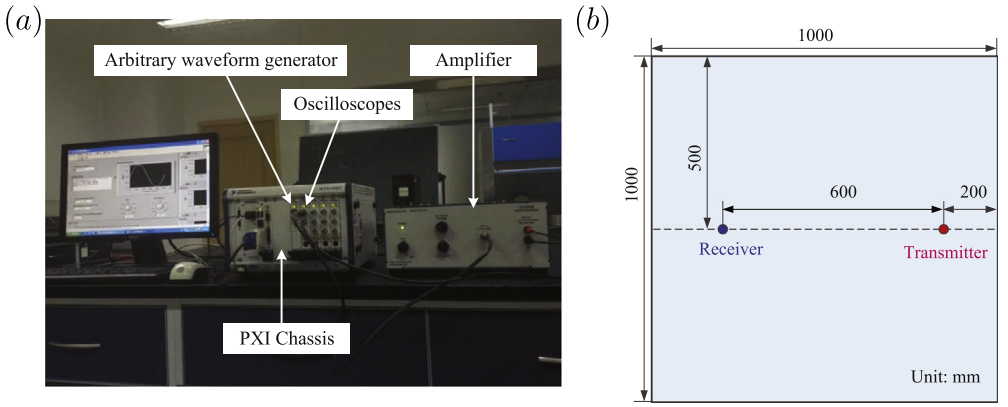

Fig. 11. Experimental setup and schematic diagram of the plate. (a) experimental setup; (b) schematic of the aluminum plate dimensions and transducers arrangements.

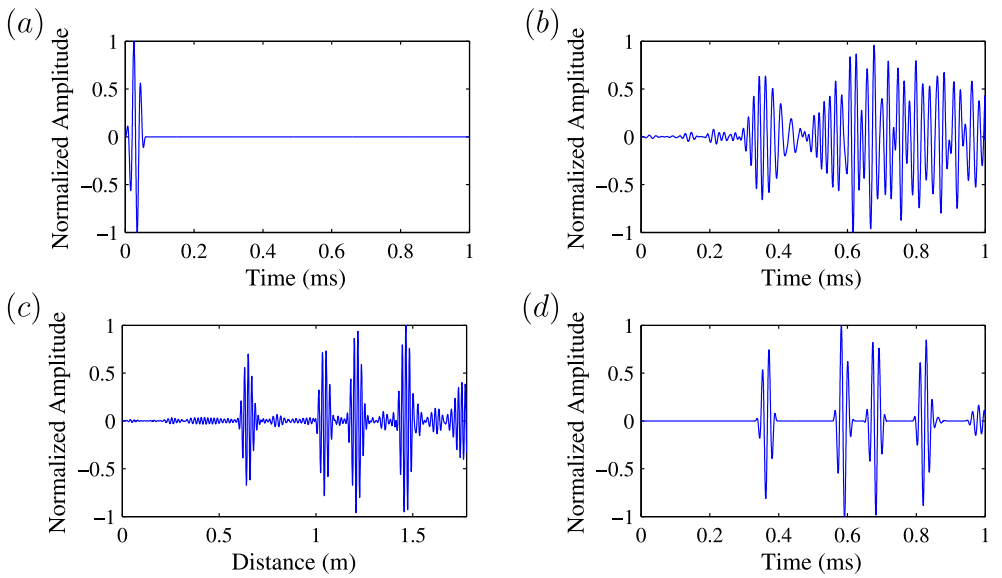

Fig. 12. Experimental results of dispersion compensation of 50 kHz A0 mode on a 2-mm 6061 aluminum plate: (a) 3-cycle Hanning-windowed tone burst excitation centered at 50 kHz; (b) the actual recorded dispersive signal; (c) compensated result using the time-distance mapping method; (d) compensated result using the developed method.

5.1. Dispersion compensation for single mode guided waves

Fig. 12 shows the dispersive signal recorded from the aluminum plate and the dispersion compensation results using the time-distance mapping and the developed methods. Fig. 12(a) shows the excitation, which is a 3-cycle Hanning-windowed tone burst centered at 50 kHz. From the recorded dispersive signal, the reflections from the boundaries overlap with each other, as shown in Fig. 12(b). The compensated results obtained by the time-distance mapping and the developed methods are presented in Fig. 12(c) and (d), respectively. The developed method can compensate each wave packet to 3 cycles, the same with the excitation. Although the time-distance mapping method can compensate the signal so that the reflections are separated in distance domain, the compensated wave packets are changed and contain higher frequency components with respect to the excitation. The results indicate that the developed method has the capability to deal with the case of single mode for dispersion compensation, and achieves better performance compared with the time-distance mapping method.

5.2. Dispersion compensation for multi-mode guided waves

In order to validate the capability of the developed method to deal with multi-mode signals, a 3-cycle Hanning-windowed tone burst excitation centered at 150 kHz, as shown in Fig. 13(a), is excited on the aluminum plate. The recorded signal contains A0 and S0 modes guided waves, as shown in Fig. 13(b). The compensated results using the time-distance mapping method with A0 and S0 dispersion curves are shown in Fig. 13(c) and (d), respectively. The compensated results of the S0 mode components are more dispersive than the original recorded signal when used the A0 mode dispersion curves for compensation. When used the S0 mode dispersion curves for compensation, the A0 mode component cannot be compensated completely. What is worse, there is disturbance near $x = 0$, as shown in Fig. 13(d). Fig. 13(e) shows the result using the developed method. All wave packets are compensated completely including components of the S0 mode direct arrival, S0 mode reflections from right/left boundary, A0 mode direct arrival, and S0 mode reflections from top/bottom

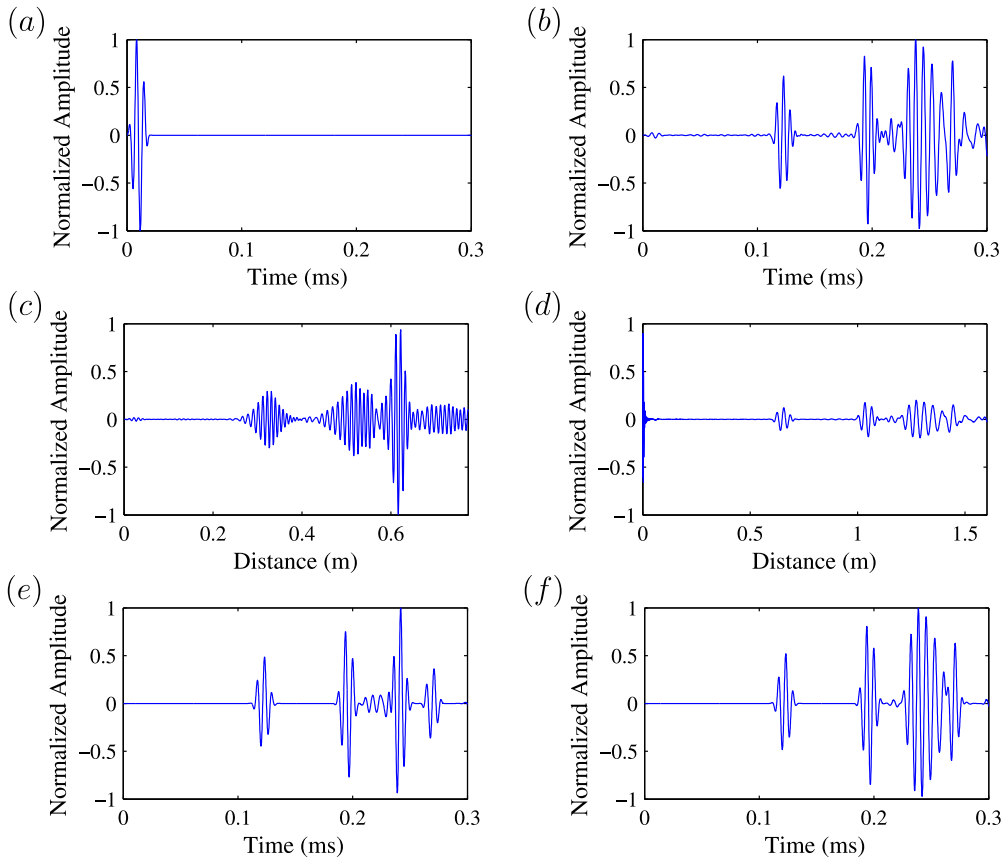

Fig. 13. Experimental results of dispersion compensation of 150 kHz A0/S0 modes on a 2-mm 6061 aluminum plate: (a) 3-cycle Hanning-windowed tone burst excitation centered at 150 kHz; (b) the actual recorded dispersive signal; (c) compensated result using the time-distance mapping method with A0 mode dispersion curves; (d) compensated result using the time-distance mapping method with S0 mode dispersion curves; (e) compensated result of the developed method using multi-mode (A0 and S0) dispersion dictionary; (f) the compensated result of the developed method using only S0 dispersion dictionary.

boundary(corresponding to the four wave packets in Fig. 13(e) from left to right). All components are compensated to 3 cycles, the same with the excitation, using the developed method. The result validates that the developed method has the capability to deal with multi-mode cases for guided wave dispersion compensation.

The dispersive signal will not be completely compensated when a dispersive signal is not completely covered by the dispersion dictionary. As an example, the dispersion compensation performance is shown in the case of that the dispersive signal is not completely covered by the dispersion dictionary with experimental data. The multi-mode dispersive signal used here is the same as the above one, as shown in Fig. 13(b). The compensated result is shown in Fig. 13(f) when only the S0 mode component is covered in the dispersion dictionary. As the result shows, the dispersive effect is hardly improved because that only the S0 mode component in the dispersive signal is compensated while the A0 mode component is not. Therefore, in the case of dispersion compensation for multi-mode guided wave, all mode components of the dispersive signal should be covered by the dispersion dictionary.

6. Conclusions

A dispersion compensation method for both single mode and multi-mode guided waves has been presented in this paper. The results of both numerical simulation and experimental verification verify the effectiveness of the developed method. The corresponding results by the time-distance mapping method are also presented as comparisons. Several conclusions can be obtained as follows.

1) The developed method can compensate both single mode and multi-mode dispersive guided waves effectively based on the accurate dispersion curves.
2) The developed method, as well as the time-distance mapping method, is sensitive to the perturbation of the dispersive curves, especially the frequency perturbation.
3) The developed method can compensate every dispersive wave packet to the waveform of the excitation well, and achieve better performance compared with the time-distance mapping method.

Acknowledgment

This work is supported by the National Natural Science Foundation of China (Nos. 51405369 and 51605365), the National Key Basic Research Program of China (No. 2015CB057400), the National Natural Science Foundation of Shaanxi Province (No. 2016JQ5049), the Young Talent fund of University Association for Science and Technology in Shaanxi of China, and the Fundamental Research Funds for the Central Universities (No. xjj2014107).

References

[1] D.E. Chimenti, Guided waves in plates and their use in materials characterization, Appl. Mech. Rev. 50 (1997) 247–284.
[2] Z. Sun, B. Rocha, K. Wu, N. Mrad, A methodological review of piezoelectric based acoustic wave generation and detection techniques for structural health monitoring, Int. J. Aerospace Eng. 2013 (2013) 1–22.
[3] Z. Su, L. Ye, Y. Lu, Guided lamb waves for identification of damage in composite structures: a review, J. Sound Vib. 295 (2006) 753–780.
[4] A.J. Croxford, P.D. Wilcox, B.W. Drinkwater, G. Konstantinidis, Strategies for guided-wave structural health monitoring, Proc. Roy. Soc. A-Math. Phys. 463 (2007) 2961–2981.
[5] M. Mitra, S. Gopalakrishnan, Guided wave based structural health monitoring: a review, Smart Mater. Struct. 25 (2016) 53001.
[6] F. Li, G. Meng, L. Ye, Y. Lu, K. Kageyama, Dispersion analysis of lamb waves and damage detection for aluminum structures using ridge in the time-scale domain, Meas. Sci. Technol. 20 (2009) 95704.
[7] R.M. Levine, J.E. Michaels, Model-based imaging of damage with lamb waves via sparse reconstruction, J. Acoust. Soc. Am. 133 (2013) 1525.
[8] A. Velichko, P.D. Wilcox, Post-processing of guided wave array data for high resolution pipe inspection, J. Acoust. Soc. Am. 126 (2009) 2973–2982.
[9] T. Wandowski, P. Malinowski, P. Kudela, W. Ostachowicz, Guided wave-based detection of delamination and matrix cracking in composite laminates, Proc. Inst. Mech. Eng. C-J. Mec. 225 (2011) 123–131.
[10] H. Zuo, Z. Yang, Y. Sun, C. Xu, X. Chen, Wave propagation of laminated composite plates via gpu-based wavelet finite element method, Sci. China Technol. Sci. (2017).
[11] H. Zuo, Z. Yang, X. Chen, Y. Xie, H. Miao, Analysis of laminated composite plates using wavelet finite element method and higher-order plate theory, Compos. Struct. 131 (2015) 248–258.
[12] C.H. Wang, J.T. Rose, F. Chang, A synthetic time-reversal imaging method for structural health monitoring, Smart Mater. Struct. 13 (2004) 415–423.
[13] J.S. Hall, J.E. Michaels, Minimum variance ultrasonic imaging applied to an in situ sparse guided wave array, IEEE Trans. Ultrason. Ferroelectr. Freq. Control 57 (2010) 2311–2323.
[14] F. Li, Z. Su, L. Ye, G. Meng, A correlation filtering-based matching pursuit (cf-mp) for damage identification using lamb waves, Smart Mater. Struct. 15 (2006) 1585–1594.
[15] W. Dong, Y. Lin, S. Zhongqing, L. Ye, L. Fucai, M. Guang, Probabilistic damage identification based on correlation analysis using guided wave signals in aluminum plates, Struct. Health Monit. 9 (2010) 133–144.
[16] T. Wandowski, P.H. Malinowski, W.M. Ostachowicz, Circular sensing networks for guided waves based structural health monitoring, Mech. Syst. Signal Procss. 66-67 (2016) 248–267.
[17] Z. Su, L. Ye, Selective generation of lamb wave modes and their propagation characteristics in defective composite laminates, Proc. Inst. Mech. Eng. L-J. Mater. 218 (2004) 95–110.
[18] K. Xu, D. Ta, W. Wang, Multiridge-based analysis for separating individual modes from multimodal guided wave signals in long bones, IEEE Trans. Ultrason. Ferroelectr. Freq. Control 57 (2010) 2480–2490.
[19] K. Xu, D. Ta, P. Moilanen, W. Wang, Mode separation of lamb waves based on dispersion compensation method, J. Acoust. Soc. Am. 131 (2012) 2714–2722.

[20] V. Giurgiutiu, Tuned lamb wave excitation and detection with piezoelectric wafer active sensors for structural health monitoring, J. Intell. Mater. Syst. Struct. 16 (2005) 291–305.
[21] P.D. Wilcox, A rapid signal processing technique to remove the effect of dispersion from guided wave signals, IEEE Trans. Ultrason. Ferroelectr. Freq. Control 50 (2003) 419–427.
[22] L. Liu, F.G. Yuan, A linear mapping technique for dispersion removal of lamb waves, Struct. Health Monit. 9 (2010) 75–86.
[23] L. De Marchi, A. Marzani, S. Caporale, N. Speciale, Ultrasonic guided-waves characterization with warped frequency transforms, IEEE Trans. Ultrason. Ferroelectr. Freq. Control 56 (2009) 2232–2240.
[24] L. De Marchi, A. Perelli, A. Marzani, A signal processing approach to exploit chirp excitation in lamb wave defect detection and localization procedures, Mech. Syst. Signal Process. 39 (2013) 20–31.
[25] S. Fu, L. Shi, Y. Zhou, J. Cai, Dispersion compensation in lamb wave defect detection with step-pulse excitation and warped frequency transform, IEEE Trans. Ultrason. Ferroelectr. Freq. Control 61 (2014) 2075–2088.
[26] B.X.L.Y. Giurgiutiu, Lamb wave dispersion compensation in piezoelectric wafer active sensor phased-array applications, SPIE (2007).
[27] Z. Luo, L. Zeng, J. Lin, J. Hua, A reshaped excitation regenerating and mapping method for waveform correction in lamb waves dispersion compensation, Smart Mater. Struct. 26 (2017) 25016.
[28] D.L. Donoho, For most large underdetermined systems of equations, the minimal l(1)-norm near-solution approximates the sparsest near-solution, Commun. Pure Appl. Math. 59 (2006) 907–934.
[29] D.L. Donoho, Compressed sensing, IEEE Trans. Inform. Theory 52 (2006) 1289–1306.
[30] E. Mor, A. Azoulay, M. Aladjem, A matching pursuit method for approximating overlapping ultrasonic echoes, IEEE Trans. Ultrason. Ferroelectr. Freq. Control 57 (2010) 1996–2004.
[31] P.W. Tse, X. Wang, Characterization of pipeline defect in guided-waves based inspection through matching pursuit with the optimized dictionary, NDT&E Int. 54 (2013) 171–182.
[32] J.B. Harley, J.M.F. Moura, Dispersion curve recovery with orthogonal matching pursuit, J. Acoust. Soc. Am. 137 (2015) L1–L7.
[33] O. Mesnil, M. Ruzzene, Sparse wavefield reconstruction and source detection using compressed sensing, Ultrasonics 67 (2016) 94–104.
[34] A. Perelli, T. Di Ianni, A. Marzani, L. De Marchi, G. Masetti, Model-based compressive sensing for damage localization in lamb wave inspection, IEEE Trans. Ultrason. Ferroelectr. Freq. Control 60 (2013) 2089–2097.
[35] A. Perelli, L. De Marchi, L. Flamigni, A. Marzani, G. Masetti, Best basis compressive sensing of guided waves in structural health monitoring, Digit. Signal Process. 42 (2015) 35–42.
[36] L. De Marchi, M. Ruzzene, B. Xu, E. Baravelli, N. Speciale, Warped basis pursuit for damage detection using lamb waves, IEEE Trans. Ultrason. Ferroelectr. Freq. Control 57 (2010) 2734–2741.
[37] S. Chen, D.L. Donoho, M.A. Saunders, Atomic decomposition by basis pursuit, SIAM J. Sci. Comput. 20 (1998) 33–61.
[38] E. van den Berg, M.P. Friedlander, Probing the pareto frontier for basis pursuit solutions, SIAM J. Sci. Comput. 31 (2008) 890–912.
[39] E. van den Berg, M.P. Friedlander, Sparse optimization with least-squares constraints, SIAM J. Optimiz. 21 (2011) 1201–1229.
[40] M.V. Afonso, J.M. Bioucas-Dias, M.A.T. Figueiredo, Fast image recovery using variable splitting and constrained optimization, IEEE Trans. Image Process. 19 (2010) 2345–2356.
[41] M.V. Afonso, J.M. Bioucas-Dias, M.A.T. Figueiredo, An augmented lagrangian approach to the constrained optimization formulation of imaging inverse problems, IEEE Trans. Image Process. 20 (2011) 681–695.
[42] M. Lowe, Matrix techniques for modeling ultrasonic-waves in multilayered media, IEEE Trans. Ultrason. Ferroelectr. Freq. Control 42 (1995) 525–542.
[43] B. Xu, V. Giurgiutiu, Single mode tuning effects on lamb wave time reversal with piezoelectric wafer active sensors for structural health monitoring, J. Nondestruct. Eval. 26 (2007) 123–134.